Jour. Geol. Soc. India (2022) 98:1505-1512
https://doi.org/10.1007/s12594-022-2205-9

ORIGINAL ARTICLE

Spectroscopic Investigations and Mineral Chemistry of Dunite from the Sargur Supracrustals (3 Ga) Greenstone Belt: Implications to Terrestrial Analogues for Lunar and Martian Dunite

Bhaskar J. Saikia[1*], Sampriti Basak[2], Rashmi R. Borah[3] and G. Parthasarathy[4!]

[1]Department of Physics, Anandaram Dhekial Phookan College, Nagaon - 782 002, India
[2]Department of Geosciences and Natural Resource Management, University of Copenhagen, 1350 Copenhagen K, Denmark
[3] Department of Physics, Nowgong College (Autonomous), Nagaon - 782 001, India
[4]National Institute of Advanced Studies, School of Natural Sciences and Engineering, Indian Institute of Science Campus, Bengaluru - 560 012, India
E-mail: *vaskaradp@gmail.com**; partha.nias@gmail.com!*

Received: 17 July 2022 / Revised form Accepted: 9 August 2022

ABSTRACT

Archean Serpentinised dunite is important not only for understanding the evolution of the ultramafic deposit of magnesium, but also serves as a possible sink material for the carbon dioxide sequestration. Future anti-pollution measures may include sequestering of waste CO_2 as magnesite ($MgCO_3$) by processing ultramafic rocks to obtain reactable Mg. For the first time, the Raman spectroscopic investigation of dunite is presented from the Karya, Sargur supracrustals (3Ga) Greenstone Belt. The Raman spectra of the sample reveal abundant presence of serpentine. Polymorphs of serpentine: lizardite, antigorite and chrysotile exhibit typical intense band at 685–692 cm^{-1} in the Raman spectrum. The Raman peaks in this study also indicates the presence of chromite and magnesite. The lunar dunite 72415, one of the oldest lunar samples of the Mg-suite, contains chromite symplectites indicative of crystallization at 40–50 km rather than at a shallow depth of <1 km, also having a olivine content of about 85%. The present study showed the dunite has about 85% olivine, which is almost identical to the Martian dunite, meteorite Northwest Africa (NWA) 2737 is the second known chassignite, an olivine-rich igneous rock with mineral compositions and isotopic ratios that suggest it formed on Mars. NWA 2737 consists of ~ 85% vol. The present study on the Karya dunite of Sargur supracrustals (3 Ga) greenstone belt, Western Dharwar Craton Karnataka, indicates a possibility of using this as a terrestrial analogue material for improving the Martian surface mineralogy and occurrence of hydrous minerals and life support system in Mars.

INTRODUCTION

Dunite is mainly obtained as an incidental product during mining of magnesite. Dunite is well-suited as a refractory material due to its low and uniform coefficient of thermal expansion. Besides, dunite exhibits properties such as, good resistance to thermal shock; spalling and slag attack; and resistance to metal attack. Dunite, calcined in rotary kilns at 1,650°C increases its refractory and foundry applications. Other uses of olivine are as loose-grain shot blasting abrasive, filtration media, in mineral wool production, filler in speciality paints, asphalt, mastics and weighing agent in concrete oil production platforms. Olivine also contributes magnesia and iron as nutrients to the soil. Dunite is a greenish-black rock and is monomineralic almost entirely made up of olivine. Dunite formation takes place in conditions that are dense or almost dense (at high temperatures) in a magma and before it cools to a particular temperature, the rock is ready to unite to form a binding anhedral olivine mass (Koukouzasa et al. 2009). Its mineral accessories include chromites, magnetite, limonite, and spinel. (Mohanty, 2009; Abdel-Karim et al. 2014). Olivine is typically one of the first minerals to crystallize from a mafic magma, and its composition is indicative of the composition and degree of evolution of the source region in the case of a primary magma, suggest that olivine is exposed largely in and around the rims of large lunar impact basins (Yamamoto et al. 2010). Such regions should represent some of the deepest materials excavated by the basin forming impact and may represent exposures of the lunar mantle, but could also represent differentiated plutons resulting from secondary magmatic intrusions into the lunar crust (Haggerty, 1973; Isaacson et al. 2011, 2014; Pieters et al. 2011, 2014; Bhattacahrya et al. 2012, 2013, 2015; Das et al. 2020; Pathak et al. 2021; Sarkar et al. 2019, 2022). Olivine is one of the most common minerals in the mafic bodies of the earth and also been identified on the surface of the Moon, Mars, and comets. Brown et al. (2021) have shown that the olivine-carbonate lithology is among the best documented rock types in 3.8 Ga Jezero crater of Martian surface (Brown et al. 2021). Olivine is typically associated with serpentine minerals [$(Mg, Fe, Ni, Mn, Zn)_{2-3}(Si, Al, Fe)_2O_5(OH)_4$] form where peridotite, dunite and other ultramafic rocks undergo hydrothermal metamorphism. Basically serpentine minerals are hydrous phyllosilicates with ~13 wt% of water. During hydrothermal metamorphism, the alterations of original rock with water near the surface of the earth or in the upper part of the mantle during subduction events, anhydrous ultramafic rocks become more hydrous, and the Ca content decreases relative to the original rocks, result in an enrichment of Mg in serpentinites. Serpentinites play an important role in numerous geological settings and control the rheology of the lithosphere where aqueous fluids interact with ultramafic rocks (Guillot

and Hattori, 2013). Serpentine group of minerals (e.g. lizardite, chrysotile, and antigorite) are polymorphs of the Mg-rich hydrous phyllosilicate with the approximate chemical formula $Mg_3Si_2O_5(OH)_4$. However, Fe, Al, and Ni may be substituted for antigorite, and Al for Si (Deer et al. 2009). Generally, lizardite, chrysotile, and antigorite are distinguished by their crystal microstructure, consisting of different arrangements of the layers. Lizardite is characterized by a flat microstructure, and chrysotile char-acterized by a curved/cylindrical crystal microstructure, while antigorite displays curvy layers resulting in a corrugated microstructure (Evans et al. 2013). These three serpentine-group minerals have different stability fields (Deer et al. 2009), particularly, lizardite is the first phase which commonly pseudomorphs after olivine; chrysotile occurs mainly as a filling in the fractures which cross-cut serpentinite rocks, whereas antigorite is considered the high-temperature phase, growing from lizardite and chrysotile with increasing grade of metamorphism at temperatures above about 320°C (Evans et al. 2013). Lizardite and chrysotile are the major components of pseudomorphic textures observed in low-grade serpentinites such as those found in oceanic lithosphere or low metamorphic grade ophiolites. Chrysotile is one of the main constituent of commercial asbestos, which was used ex-tensively for thermal and electric insulation (Fubini and Fenoglio, 2007). Serpentine minerals in planetary bodies provide unambiguous evidence of presence of water on the planetary bodies. Hence the micro-Raman spectroscopic studies on serpentinised dunite provide an insight for improving the understanding of the planetary mineralogy. Raman spectroscopy is a non-destructive rapid experimental technique that permits the identification of mineral species without long and costly preparation of the sample (Saikia et al. 2021, 2022a,b,c). Raman spectroscopic technique has been used by number of earlier workers for identification and structural analysis of serpentine-group minerals (lizardite, chrysotile and antigorite) (e.g., Pasteris and Wopenka, 1987; Lewis and Griffiths, 1996; Bard et al. 1997; Kloprogge and Frost, 1999; Auzende et al. 2004; Guillot and Hattori, 2013; Petriglieri et al. 2015). Recently Mars Rover Mission 2020 also employed Raman spectroscopy for planetary exploration. The Scanning Habitable Environments with Raman and Luminescence for Organics and Chemicals (SHERLOC) is an arm-mounted, Deep UV (DUV) resonance Raman and fluorescence spectrometer utilizing a 248.6-nm DUV laser and <100 micron spot size for detecting possible organics and hydrocarbons on Martian surface. The laser is integrated to an auto-focusing/scanning optical system, and co-boresighted to a context imager with a spatial resolution of 30 µm. Deep UV-induced native fluorescence is very sensitive to condensed carbon and aromatic organics, enabling detection at or below 10-6 w/w (1 ppm) at <100 µm spatial scales. SHERLOC's deep ultra-violet resonance Raman enables detection and classification of aromatic and aliphatic organics with sensitivities of 10-2 to below 10-4 w/w at <100 µm spatial scales (https://mars.nasa.gov/mars2020). In order to explore the possibility of providing yet another terrestrial analogue material from India we undertook investigation on the characterization of Archean dunite identify the water bearing mantle minerals using micro Raman spectroscopic technique.

GEOLOGICAL SETTINGS

The Dharwar craton in southern India is a natural laboratory as it preserves one of the earliest continental crustal records in the world covering a time span of over 3.3 Ga (Devaraju et al. 2009). On the basis of age, type of rocks and abundance of greenstone belts, it is subdivided into two components (Fig.1), namely the western Dharwar craton (WDC) and eastern Dharwar craton (EDC). The two subcomponents are divided by a ~500 km long N-S trending intrusive body of alkali-feldspar rich Closepet granite (~2.5 Ga; Taylor et al. 1998). There is a progressive increase in the grade of metamorphism from north to south in the Dhawar craton which is often interpreted as a tilted crustal sequence of varied depths. The southern margin of the Dharwar craton is bounded by the higher grade metamorphosed rocks of the southern granulite terrain (SGT).

Two major supracrustal units are located in the WDC: (i) the Sargur supracrustals that comprises the older greenstone belt with a recorded age between ~3.4-3.1Ga (Datta and Mondal, 2021 and references therein) and (ii) the Dharwar Supergroup, known as the younger

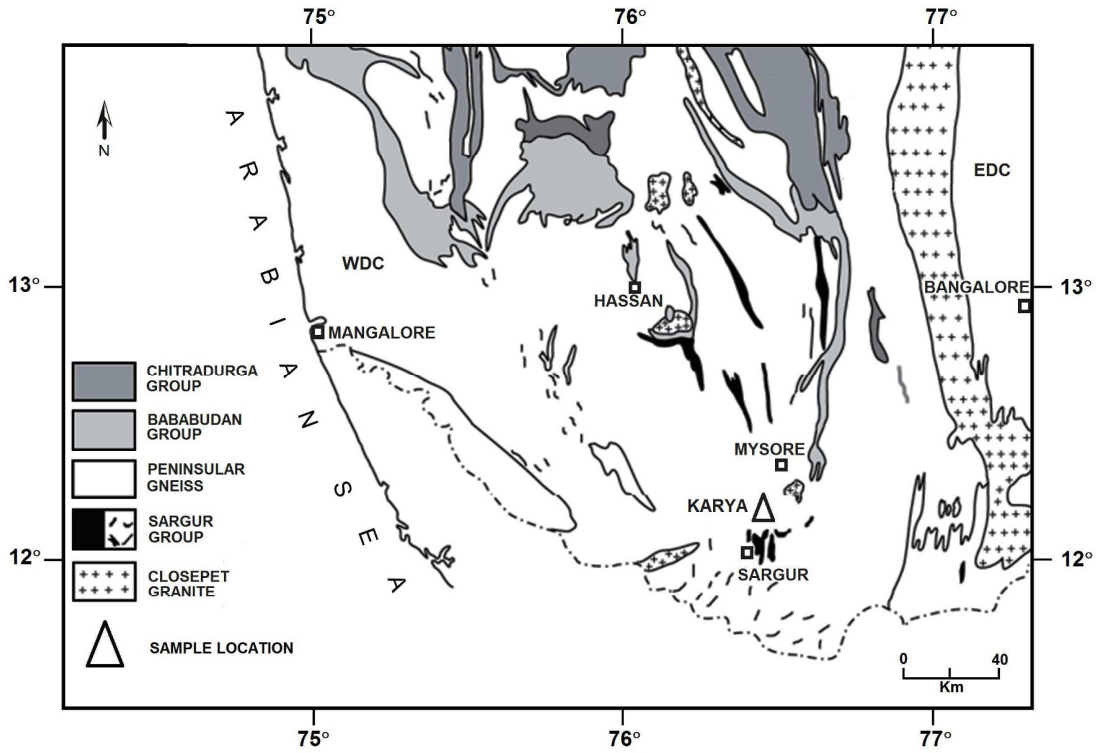

Fig. 1. Geological map of Mysore, Peninsular India. Triangle in the diagram indicates area under study (modified after Rao et al. 1975).

greenstone belt (~ 2.9–2.7Ga; Taylor et al. 1988). The Dharwar Supergroup (namely the Bababudhan, Shimoga and Chitradurga group) overlies the basement tonalite-trondhjemite-granodiorite (TTG) suite. The major rock type of the Sargur supracrustals are metavolcanics (which includes komatiites, komatiitic basalts and basalts) and metasediments (graphite-garnet-kyanite-sillimanite-muscovite bearing schists along with quartzite, banded iron formation and carbonate) and they occur as enclaves in the Archean granodioritic gneissic rocks (Janardhan and Srikantappa, 1975; Srikantappa et al. 1984, 1985; Mondal et al., 2008; Mukherjee et al. 2012; Mukherjee et al. 2014; Datta and Mondal, 2021).

The studied dunite sample belongs to the serpentinised ultramafic bodies which occurs as enclave within the Archean TTG gneissic complex and belongs to the Sargur supracrustals. The ultramafics which includes peridotites, serpentinised dunites, amphibolites and pyroxenites are known as Alpine type ultramfics together with the gneisses, metavolcanics and metasediments forms an 'en echelon' belt of almost 320 km long (Rao et al. 1975) and occupies the axial zones of the Dharwar anticlinorium (Pichamuthu, 1962). The dunite bodies often hosts amphibolites and are cut across by magnesite veins. These magnesite bodies are mined at several locations for example, the currently abandoned Dodkanya mine site or the active Karya mine site. The contact between the ultramafics and the gneisses are sharp and are represented by talc schist lithology (Fig.1). The following reasons based on field relationships attests to the older origin of the dunites in comparison to the Peninsular gneiss (Rao et al. 1975): (a) the Peninsular gneiss hosts the enclaves of the dunites within (b) Veins of Peninsular gneiss cross cuts the dunite bodies (c) Regional schistosity runs parallel to the schistosity in the associated pyroxenites and dunites (d) absence of any high temperature metamorphic signature in the gneisses due to the intrusion of the ultramafics (e) presence of a deeper and larger ultramafic root below the gneissic rock as suggested by gravity studies (Qureshy et al. 1970).

Site Location and Accessibility

The studied dunite sample was from Karya mine, Karya near Nanjangud Town (Longitude E: 76°32'47.3" - E: 76°033'20.2" Latitude N: 12°04'33.0" - N: 12°3'59.3"). The fresh dunite sample was kindly provided by Late Professor B. P. Radhakrishna. The Karya Magnesite Mine, its existing production is 0.24 lakh tonnes per annum with open cast mining method and having more demand in the market and also associated with dunite having commercial value. In view of the same, Mysuru Minerals Limited, Government of Karnataka proposes to increase its production from 0.24 lakh tonnes per annum to 3.875 lakh tonnes per annum at Karya village, Nanjangud taluk, Mysuru district, Karnataka.

Experimental Techniques

The Raman spectra were collected on bulk dunite sample using a Nd: YAG laser with a power of ~5 mW, which used an excitation source having a wavelength of 532 nm coupled with a Jobin-Yvon Horiba LabRam-HR Micro-Raman spectrometer (Horiba Scientific, USA) equipped with an Olympus microscope with 109, 509, and 1009 objectives. A motorized x–y stage is included in this arrangement and used 1800 grooves mm^{-1} grating in the range from 100 to 3000 cm^{-1}. A silicon wafer (520.7 ± 0.5 cm^{-1}) was applied for calibration. The excellent accuracy (±0.5 cm^{-1}) and precision (±0.1 cm^{-1}) of peak positions for this instrument over the whole Raman spectral range make it relatively straightforward to use this technique to identify minerals based on their spectral signatures. An edge filter was used for measuring the exact Stokes lines. The data interpretation procedure used a Gaussian fit to find the exact position of the maximum of each peak. Minerals were identified by comparing the band positions in our spectra with the Raman data on the end member minerals at ambient pressure and temperature conditions (RRUFF-database http://rruff.info). Raman data were collected at room temperature (30 °C). Spectra were collected with counting times ranging between 10 and 60 s. Powder methods are more reliable for characterization of mineral phases. The composition of the dunite sample was also determined by the X-ray diffraction technique (XRD) using PHILIPS PW 3710/31 diffractometer, scintillation counter, CuKQ radiation and Ni filter at 40 kV and 35 mA (Philips, USA). This instrument is connected to a computer system using APD program and PDF-2 database for mineral identification. We used a 2θ range of 10–80° with a step size of 0.02° and a 0.5 s count time per step. The slits used consisted of 1° fixed divergence and anti scatter slits and a 0.2 mm receiving slit.

RESULTS AND DISCUSSIONS

The modal composition of the dunite samples determined by optical petrological microscope (in vol%) of the studied dunite rock sample consisted mainly of 85.2 % olivine, chromite (3.0%), low Ca-pyroxene (2%) and phyllosilicates (9%) and other opaque minerals (1%). The uncertainties involved is typically ±0.05%. The x-ray diffraction pattern showed mixed peaks and elucidates the main rock-forming minerals to be olivine (forsterite) with some additional peaks corresponding to magnesite and serpentine mineral group: lizardite and antigorite.

Figure 2 shows the XRD patterns for the studied sample as well as the reference patterns for dunite, lizardite, antigorite, magnesite ($MgCO_3$) and SiO_2. The presence of serpentinite minerals testifies a prominent alteration of olivine and serpentinization of the dunite rock. This is confirmed by the large value of loss on ignition of 10.42 wt% and low silicate ratio of 1.34, which corresponds to forsterite 1.34. The chemical composition of studied dunite rock is reported in Table 1. The magnesite content of the studied sample can be due to

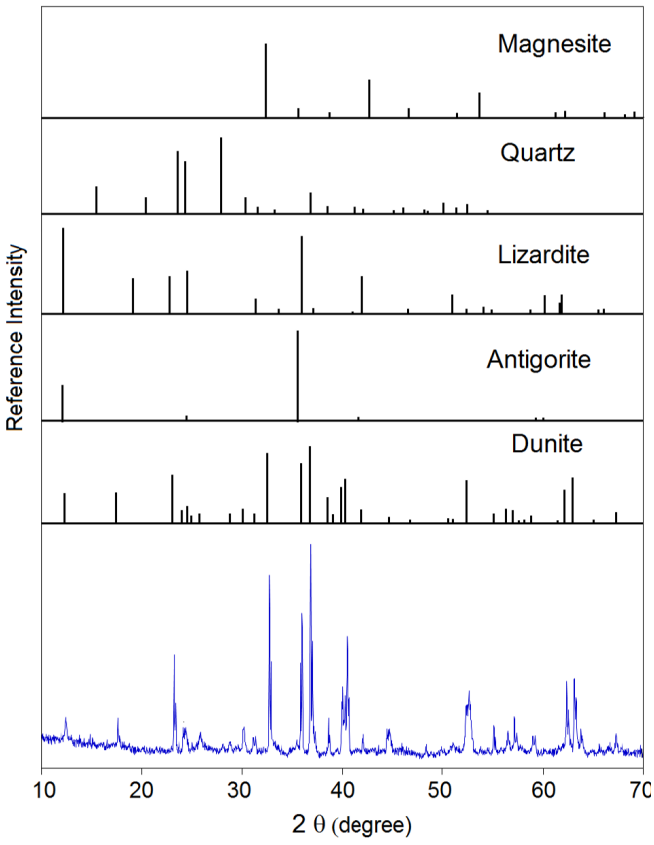

Fig. 2. X-ray diffraction (XRD) of magnesite, quartz, lizardite, antigorite and dunite with the studied sample.

Table 1. The chemical composition of studied dunite rock.

Compound	MgO	SiO_2	FeO	Al_2O_3	MnO	CaO	Na_2O	K_2O	Total
	52.38	33.87	11.84	0.69	0.17	0.99	0.05	0.01	100
Wt%	51.99	33.85	12.16	0.81	0.16	0.97	0.05	0.01	100
	52.29	33.75	11.97	0.77	0.18	0.96	0.06	0.02	100

intense serpentinization of rocks under hydrothermal and hydrothermal-contact alteration of ultrabasic rocks. Powder XRD data on the dunite sample has been interpreted in a similar way of characterization of mineral phases of meteorite samples (Dunn et al. 2010; Saikia et al. 2022a). For XRD peaks of individual minerals we also referred the Ruff database (https://rruff.info/Olivine/R100103).

Figure 3 (a-b) shows the presence of olivine and pyroxene in the studied sample. Raman peaks in the range 700-1100 cm^{-1} are attributed to the internal stretching vibrational modes of the SiO_4 tetrahedra. In this region, the renowned doublet is found for the Si-O symmetric stretching bands at 813-824 cm^{-1} and 852-857 cm^{-1}, and a medium wave number anti-symmetric Si-O stretching band appears at 960-965 cm^{-1} due to fosterite (F_o). Fig. 3(a) exhibits the well-known Raman doublet at 823 cm^{-1} and 855 cm^{-1} with the anti-symmetric Si-O stretching band at 962 cm^{-1}. The characteristic Raman doublet found at 823 cm^{-1} and 855 cm^{-1} from the coupling between the symmetric ($v1$) and anti-symmetric ($v3$) stretching modes of Si-O_{nb} bonds in SiO_4

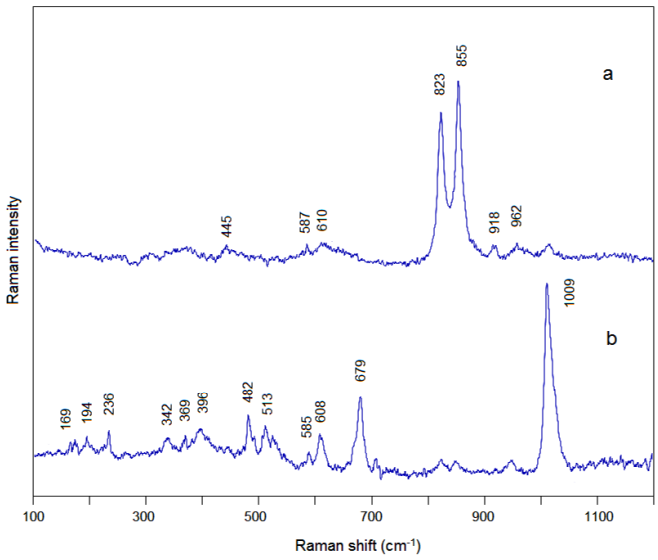

Fig. 3. Raman spectra show the presence of olivine and pyroxene in the studied sample in the region 100-1200 cm^{-1}.

tetrahedra of olivine (Saikia et al. 2017a,b,c). At the Raman spectra of olivine, the band position and the relative intensities of the characteristic SiO_4 stretching doublet are sensitive to the cation substitution. The variation of the doublet positions due to the cation substitutions can be observed. Using the correlation charts between the positions of this doublet, they correspond to forsteritic olivines (Chopelas 1991). The Raman doublet positions are used to calculate the F_o of olivine grains in our sample applying the formula of Kuebler et al. (2006).

$$Fo\ (BD1\ \&\ BD2) = y_3 + a_3x_1 + b_3x_2 + c_3x_1^2 + d_3x_2^2$$

where x_1 is the *DB1* peak position, x_2 is the *DB2* peak position, y_3 is the intercept, and a_3, b_3, c_3, and d_3 are the coefficients listed in Table 4 of Kuebler et al. (2006). The calculated F_o value 91, is in good agreement with the chemical compositions obtained by electron microprobe analysis.

In pyroxenes, the peaks in the 800–1100 cm^{-1} region are generally assigned to Si-O stretching vibrations related to the non-bridging Si-O bonds; the Si-O bending modes at 500-590 cm^{-1}; and metal-oxygen bending and stretching modes are observed below 600 cm^{-1}. The wavenumber of the Si-O stretching modes of the bridging O atoms (Si-O_{br}) is assigned to be in the range 650–750 cm^{-1}(Huang et al. 2000). The most intense bands at 1009 cm^{-1} and 679 cm^{-1} (Fig.3b) have been assigned to the stretching non-bonded oxygen (Si–O_{nb}) and chain-bonded oxygen (Si–O_b–Si) of the SiO_4 tetrahedra, respectively, in two oxygen shared SiO_4 tetrahedra of inosilicates (Chopelas 1991; Saikia et al. 2017a,b; 2018). The characteristic A_g vibrational mode of plagioclase feldspar is observed in the spectrum at 513 cm^{-1} with a second peak at 482 cm^{-1}, both peaks have been assigned to a mixed Si–O–Si (or Si–O–Al) band/stretch (Mernagh and Liu 1991). The Si-O banding modes are found at 585 and 608 cm^{-1}. Below 400cm $^{-1}$ region, the Raman peaks at 236, 342, 369, 396 cm^{-1} are mostly contributed by lattice modes: rotations and translations of SiO_4 units and translations of octahedral cations (Mg^{2+}, Fe^{2+}) in the crystal lattice (Chopelas 1991). These peaks can provide important information about temperature dependence but the intensities of these peaks are low owing to the polarizabilities of the octahedral structural units (Hofmeister et al. 1989; Chopelas 1990, 1991).

Figure 4(a-b) indicates the presence of both chromite and magnesite peaks in the spectrum together with olivine doublets at 823-824 cm^{-1} and 853-856 cm^{-1}. This can happen when the analyses are performed on overlapped or very closely spaced fine grains, when the laser beams both grains at the same time and the laser diameter is too large. Therefore, the detector collects photons scattered from the two different minerals, resulting in a spectrum which is the mathematical sum of the two spectra of two different minerals. The strong Raman peak at 680 cm^{-1} and three weak peaks at 593, 495, and 338 cm^{-1} reveal the presence of chromite (Fig. 4a). The strongest peak at 680 cm^{-1} is assigned to the A_{1g} mode and this feature presumably generated by the bonds in (Cr^{3+}, Fe^{3+}, Al^{3+})O_6 octahedra. However, Fig.4b, shows that the spectrum of chromite is distinct from that of magnesite, which has a strong peaks at 667, 329 cm^{-1} and three weak peaks of magnesite vibration modes at 545, 407, and 215 cm^{-1} (Wang et al. 2001). Generally, it is possible to distinguish a range of minerals within the same functional group (e.g. dolomite, calcite and magnesite) from each other by the positions of the low-frequency lattice modes and the mid-frequency internal modes (Bischoff et al. 1985; McMillan and Hofmeister 1988; Sharma et al. 2002, 2003; Stopar et al., 2005). The vibrational modes of magnesite peaks are assigned as symmetric stretching (667 and 545 cm^{-1}), lattice vibration (407 cm^{-1}), librational

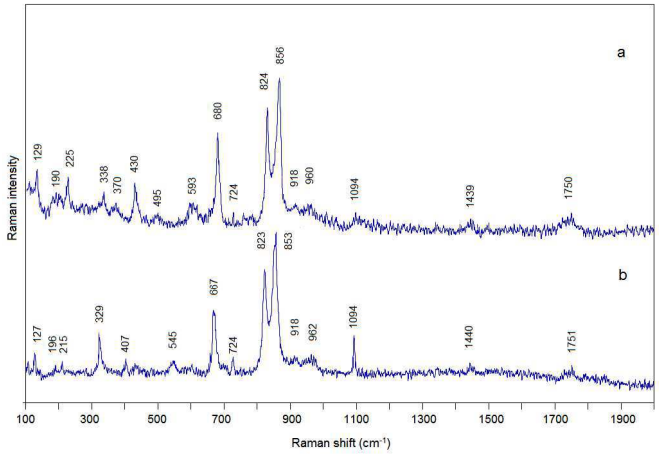

Fig. 4. Raman spectra indicate the presence of chromite and magnesite in the studied sample in the region 100-2000 cm^{-1}.

mode (329 cm^{-1}) and translational mode (215 cm^{-1}) of the $(CO_3)^{2-}$ group. The weak peaks at 724 cm^{-1} and 1439-1440 cm^{-1} found in both spectra (Fig. 4a-b) corresponds to the $\nu_4(CO_3)^{2-}$ in-plane bending mode and $\nu_3(CO_3)^{2-}$ anti-symmetric stretching mode of carbonate ions respectively. An additional weak band at 1750-1751cm^{-1} is observed in the both spectra due to an overtone mode of the infrared-active $2\nu_2(A_u)$ mode (Bischoff et al. 1985). The Raman peak at 1094 cm^{-1} is considered as the fingerprint of carbonate ions corresponding to the $\nu_1(CO_3)^{2-}$ symmetric stretching mode of carbonate oxygen atoms (Edwards et al. 2005).

Serpentine minerals are hydrous phyllosilicates with ideal end member composition $Mg_3Si_2O_5(OH)_4$ and display a layered crystal structure based on overlapped tetrahedral and octahedral sheets. Generally, they are formed by the hydration of olivine, orthopyroxene and clinopyroxene in ultramafic rocks. The principal minerals of the serpentine group: chrysotile, antigorite and lizardite, have a similar chemical composition, but significantly different structures. Polymorphs of serpentine (lizardite, antigorite and chrysotile) were exhibit typical intense band at 685–692 cm^{-1} in the Raman spectrum. The peak positions and their possible assignments are tabulated in Table 2. The systematic micro-Raman characterization of serpentine minerals, the intense band ~690 cm^{-1} in different microstructural positions indicates that Si-O_b-Si vibrations occur at about 685 cm^{-1} in antigorite, but at 688-692 cm^{-1} in both chrysotile and lizardite (Groppo et al. 2006). In Fig. 5a, the intense and weak Raman band at 690 cm^{-1} and 1095 cm^{-1} arises due to Si-O_b-Si symmetric stretching and anti-symmetric (Si-O_{nb}) stretching vibrations respectively which is indicative to lizardite (Kloprogge et al.1999; Rinaudo et al. 2003). The bending modes of SiO_4 tetrahedra occur at 390 cm^{-1} in chrysotile, while it occur between 380 and 388 cm^{-1} in lizardite (Groppo et al. 2006). The Raman peaks found at 388 and 238 cm^{-1} produced due to $SiO_4(\nu_5)$ tetrahedra modes and O-H-O group vibrations respectively and this point towards the crystallization of lizardite (Rin-audo et al. 2003). According to Groppo et al. (2006), in lizardite the band ~ 390 cm^{-1} shifts toward lower wavenumbers, with increasing amounts of Al replacing Si in the tetrahedral sites (Groppo et al. 2006). The peak at 350 cm^{-1} is related to the vibrations of SiO_4 tetrahedra (Kloprogge et al.1999). The weak band at 632 cm^{-1} is ascribed as the antisymmetric OH-Mg-OH translation modes. The weak band found at 197 cm^{-1} and 467 cm^{-1} are arise corresponds to the A_g mode of Mg $(O,OH)_6$ group vibrations and Mg-OH translations or ν_6 SiO_4 vibrations (Kloprogge et al. 1999). In Fig. 5b, Raman spectrum exhibits the occurrence of antigorite and chrysotile. The bands at 1105, 692, 629, 465, 432, 390, and 348 cm^{-1} are attributed to chrysotile, in agree-ment with the spectrum obtained by Kloprogge et al (1999), whereas the characteristic bands of antigorite occur at 1045, 519, and 382 cm^{-1}. The weak band at 519 cm^{-1} is an irregular band that based on Rinaudo et al. (2003) and Lazarev (1962) is associated to the deformation of the SiO_4–AlO_4 tetrahedra (Rinaudo et al. 2003; Lazarev 1962). On the basis of the data from Groppo et al. (2006), bands at 465 cm^{-1} can also be assigned to antigorite (Groppo et al. 2006). An intense peak of serpentine minerals exhibits ~230 cm^{-1} related to O–H–O vibrations, where O is the non-bridging oxygen atom of the tetrahedron SiO_4, and H is the hydrogen atom of the OH group tilted towards an octahedral cation vacancy (Griffith and Lesniak 1969). The strong band observed at 232 cm^{-1} may be occurred due to both antigorite and chrysotile, while the weak peak at 322 cm^{-1} arises due to chrysotile (Kloprogge et al. 1999). Generally, chlorite exhibits 546, 463, 357, and 284 cm^{-1} peak along with an intense peak at 682–683 cm^{-1} (Prieto et al. 1991). The weak peak observed at 282 cm^{-1} is attributed to chlorite. In both spectra a weak band is observed at 1045 cm^{-1} arise due to antisymmetric Si-O_b-Si stretching modes which is attributed to antigorite, because it occurs in a frequency range where no band of chrysotile or lizardite is present (Rinaudo et al. 2003; Petriglieri et al. 2015).

In the 3600–3800 cm^{-1} region the serpentine minerals have its

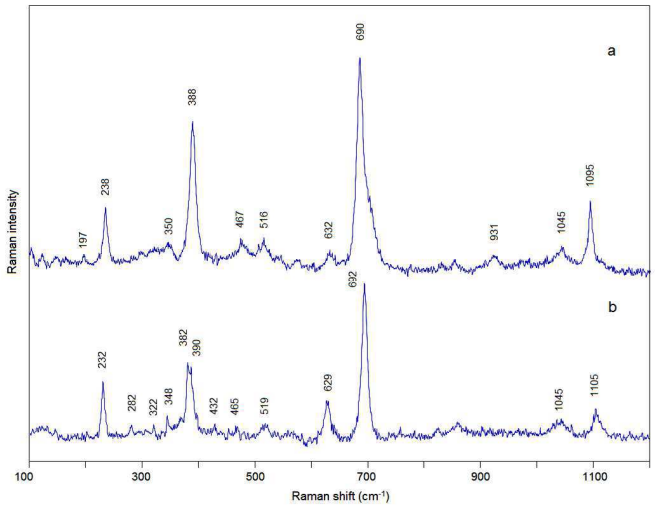

Fig. 5. Raman spectra show the polymorphs of serpentine in the studied sample in the region100-1200 cm^{-1}.

Table 2. Assignment of peaks in the Raman spectra at low-wavenumber regions of the main serpentine phases studied in this work and compared with results obtained by Groppo et al. (2006); Auzende et al. (2004); Kloprogge et al. (1999) and Rinaudo et al. (2003).

Chrysotile			Lizardite			Antigorite			This Study	Assignments
Groppo et al.	Auzende et al.	Kloprogge et al.	Groppo et al.	Auzende et al.	Rinaudo et al.	Groppo et al.	Auzende et al.	Rinaudo et al.		
-	-	199	-	-	-	-	-	-	197	A_{1g} mode of $Mg(O, OH)_6$
231	235	231	233	241	233	230	235	230	232; 238	Vibrations O-H-O
345	346	345	350	351	350	-	-	-	384; 350	Bending of SiO_4
-	-	374	-	-	-	375	377	375	-	Symmetric Mg-OH
389	391	388	388	393	388	-	-	-	382; 388; 390	Symmetric ν_5 SiO_4
-	-	432	-	-	-	-	-	-	432	Antisymmetric Mg-OH
-	-	466	-	-	-	-	-	-	465; 467	Mg-OH translation + ν_6 SiO_4
-	-	-	510	527	510	520	528	520	516; 519	SiO_4-AlO_4 deformation
620	-	622	-	-	-	-	-	-	-	Translation OH–Mg–OH
-	-	629	630	-	630	635	-	635	629; 632	Translation OH–Mg–OH
692	694	692	690	695	690	683	685	683	690; 692	ν_s Si–O_b–Si
-	-	-	-	-	-	1044	-	1044	1045	ν_{as} Si–O_b–Si
-	-	-	1096	-	-	-	-	-	1095	ν_{as} Si–O_{nb}
1105	-	1011	-	-	1096	-	-	-	1105	ν_{as} Si–O_{nb}

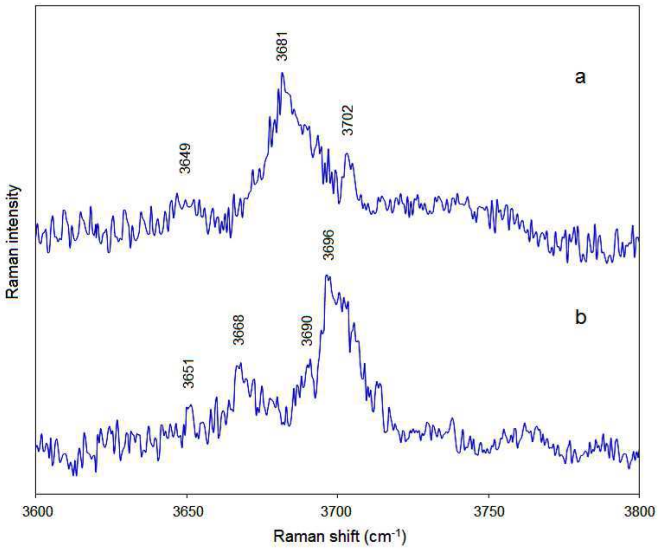

Fig. 6. Raman signature due to the inner and outer hydroxyl vibrations in the region 3600– 3800 cm^{-1}.

characteristic Raman signature due to the inner and outer hydroxyl vibrations. Titulaer et al.(1993) and Kloprogge et al.(1999) suggested the inner hydroxyl vibration occurred at a lower wavenumber than the outer hydroxyl groups (Titulaer et al. 1993; Kloprogge et al. 1999). However, O'Hanley & Dyar (1998) and Auzende et al.(2014) suggested that the lower wavenumber hydroxyl bands in lizardite are attributed to the outer hydroxyls, whereas the higher wavenumber bands are attributed to the inner hydroxyl vibration (O'Hanley and Dyar, 1998; Auzende et al. 2004). In Fig. 6a-b three main serpentine minerals (lizardite, chrysotile, and antigorite) can be distinguished. The Raman peak position (Fig. 6a) at 3681 cm^{-1} and a smaller secondary peak at 3702 cm^{-1} with a broad peak ~3649 cm^{-1} indicates lizardite (Petriglieri et al. 2015; Rooney et al. 2018). However, in Fig. 6b, the Raman peak positions at 3696 cm^{-1}, with a shoulder at 3690 cm^{-1} and a broad peak at ~3651 cm^{-1} is consistent with the Raman spectral positions of chrysotile (Groppo et al. 2006; Auzende et al. 2004; Rooney et al. 2018). According to Rooney et al.(2018), antigorite is characterised by two peaks at 3667 ± 2 cm^{-1} and 3696 ± 2 cm^{-1} (Rooney et al. 2018). The peak at 3668 cm^{-1} arises in Fig.6b due to antigorite, and the characteristic antigorite peak positions are overlapped with the characteristic chrysotile peak positions.

CONCLUSION

The Raman spectroscopy and chemical analyses, provides the sample is composed of the main phases of the serpentine group: chrysotile, lizardite, and antigorite. The occurrence of minor phases, such as carbonates, chromite, magnesite, leads to a pleasing colour variation in the sample. The results lead to an increase in the ability to predict serpentine polymorphs in dunite from Sargur supracrustals (3Ga) by exclusive use of Raman spectra of the sample. The present study showed the dunite has about 85% olivine, which is almost similar to the Martian dunite, Meteorite Northwest Africa (NWA) 2737 is the second known chassignite, an olivine-rich igneous rock with mineral compositions and isotopic ratios that suggest it formed on Mars. The present study on the Karya dunite indicates a possibility of using this as terrestrial analogue for improving the Martian surface mineralogy and occurrence of hydrous minerals and life support system in Mars.

Acknowledgement: We are grateful to Late Dr. B. P. Radhakrishna, for providing the dunite sample and his keen interest in our Mineral Chemistry work. We thank the Editor Professor B. Mahabaleshwar and the anonymous reviewers for the most constructive comments on the relevance of dunite to the planetary materials. We thank Director, Indian Institute of Technology, Guwahati (IITG) for providing Raman and powder XRD facilities for characterization of the sample. We also thank Dr. S. Sarmah, IIT Guwahati for his assistance in the micro-Raman spectroscopic analysis. One of us (GP) is grateful to National Institute of Advanced Studies, Bengaluru and Indian National Science Academy, New Delhi for their support through INSA-Senior Scientist Scheme. Dr. Sampriti Basak is grateful to the Indian Academy of Sciences, Bengaluru for the support.

References

Abdel-Karim, A.A.M., Elwan, W.I., Helmy, H., El-Shafey, S.A. (2014) Spinels, Fe-Ti oxide minerals, apatites, and carbonates hosted in the ophiolites of Eastern Desert of Egypt: Mineralogy and chemical aspects. Arab. Jour. Geosci., v.**7**(2), pp.693-709.

Auzende, A.L., Daniel, I., Reynard, B., Lemaire, C., Guyot, F. (2004) High-pressure behaviour of serpentine minerals: A Raman spectroscopic study. Phys. Chem. Miner., v.31 pp.269–277.

Bard, D., Yarwood, J., Tylee, B. (1997) Asbestos fibre identification by Raman microspectroscopy. Jour. Raman Spectrosc., v.28, pp.803–809.

Bhattacharya, S., Chauhan, P., Ajai (2012) Discovery of orthopyroxene–olivine–spinel assemblage from the lunar nearside using Chandrayaan-1 Moon Mineralogy Mapper data. Curr. Sci., v.103(1), pp.21-23.

Bhattacharya, S., Saran, S., Dagar, A., Chauhan, P., Chauhan, M., Ajai, Kumar, A. S. K. (2013) Endogenic water on the moon associated with the non-mare silicic volcanism: Implications for hydrated lunar interior. Curr. Sci., v.105(5), pp.685-691.

Bhattacharya, S., Lal, D., Chauhan, M., Chauhan, P., Ajai, Kumar, A.S.K. (2015) Detection of hydroxyl-bearing exposures of possible magmatic origin on the central peak of crater Theophilus using Chandrayaan-1 Moon Mineralogy Mapper (M3) data. Icarus, v.260, pp.167-173.

Bischoff, W. D., Sharma, S. K., Mackenzie, F. T. (1985) Carbonate ion disorder in synthetic and biogenic magnesian calcites: A Raman spectral study. Amer. Mineral., v.70, pp.581-589.

Brown, A. J., Wiens, R. C., Maurice, S., Uckert, K., Tice, M., Flannery, D., Deen, R. G., Tarnas, J. D., Treiman, A. H., Siebach, K. L., Beegle, L. W., Abbey, W. J., Bell, J. F., Johnson, J. R., Mayhew, L. E., Simon, J. I., Hurowitz, J. A., Beyssac, O., Willis, P. A., Bhartia, R., Smith, R. J., Fouchet, T., Quantin-Nataf, C. (2021) Mars2020 In Situ Investigation of Alteration at Jezero Crater. 52nd Lunar and Planetary Science Conference, 15-19 March, 2021. LPI Contribution No. 2548, id.1749.

Chopelas, A. (1990) Thermal properties offorsterite at mantle pressures derived from vibrational spectroscopy. Phys. Chem. Miner., v.17, pp.149-156.

Chopelas, A. (1991) Single crystal Raman spectra of forsterite, fayalite, and monticellite. Amer. Mineral., v.76, pp.1101–1109.

Das, S., Basu,A.R., Mukherjee, B.K., Marcantonio, F., Sen, K., Bhattacharya, S., Robert T. Gregory, R.T. (2020) Origin of Indus ophiolite-hosted ophicarbonate veins: Isotopic evidence of mixing between seawater and continental crust-derived fluid during NeoTethys closure. Chem. Geol. v.551, pp.119772.

Datta, P., Mondal, S.K. (2021) Compositional variations, thermometry, and probable parental magmas of Archean chromite from the Sargur greenstone belt, Western Dharwar Craton (India). Lithos, v.380, pp.105867.

Deer, W.A., Howie, R.A. Zussman, J. (2009) Rock forming minerals: Layered silicates excluding micas and clay minerals. Geol. Soc. London, v.3B, pp.314.

Devaraju, T.C., Viljoen, R.P., Sawkar, R.H., Sudhakara, T.L. (2009) Mafic and ultramafic magmatism and associated mineralization in the Dharwar craton, southern India. Jour. Geol. Soc. India, v.73, pp.73–100.

Dunn, T. L., Gordon, C., McSween, H.Y., McCoy, T.J. (2010) Analysis of ordinary chondrites using powder X-ray diffraction: 1. Modal mineral abundances. Meteoritics Planet Sci., v.45(1), pp.127–138.

Edwards, H.G.M., Villar, S.E.J., Jehlicka, J., Munshi, T. (2005) FT–Raman spectroscopic study of calcium-rich and magnesium-rich carbonate minerals. Spectrochim Acta A, v.61, pp.2273–2280.

Evans, B. W., Hattori, K., Baronnet, A. (2013) Serpentinite: What, why, where? Elements, v.9, pp.99–106.

Fubini B., Fenoglio, I. (2007) Toxic potential of mineral dust. Elements, v.3(3), pp.407–414.

Griffith, W. P., Lesniak, P. J. B. (1969) Raman Studies on Species in Aqueous Solutions. Part 111. Vanadates, Molybdates, and Tungstates. Jour. Chem. Soc. (A), pp.1066-1071.

Groppo, C., Rinaudo, C., Cairo, S., Gastaldi, D., Compagnoni, R.(2006) Micro-Raman spectroscopy for a quick and reliable iden-tification of serpentine minerals from ultramafics. European Jour. Mineral., v.18(3), pp. 319–329.

Guillot, S., Hattori, K. (2013) Serpentinites: Essential roles in geodynamics, arc volcanism, sustainable development, and the origin of life. Elements, v.9, pp.95–98.

Haggerty, S.E. (1973) Luna 20: mineral chemistry of spinel, pleonaste, chromite, ulvospinel, and rutile. Geochim. Cosmochim. Acta, v.37, pp.857 -867.

Hofmeister A. M., Xu J., Mao H. K., Bell P. M., Hoering T. C. (1989) Thermodynamics of Fe-Mg olivines at mantle pressures: Mid and far-infrared spectroscopy at high pressure. Amer. Mineral., v.74, pp.281–306.

Huang, E., Chen, C.H., Huang, T., Lin, E.H., Xu, J.A. (2000) Raman spectroscopic characteristics of Mg-Fe-Ca pyroxenes. Amer. Mineral., v.85, pp.473–479.

Isaacson, P.J., Pieters, C.M., Besse, S., Clark, R.N., Head, J.W., Klima, R.L., Mustard, J.F., Petro, N.E., Staid, M.I., Sunshine, J.M., Taylor, L.A. (2011) Remote compositional analysis of lunar olivine-rich lithologies with Moon Mineralogy Mapper (M3) spectra. Jour. Geophys. Res. Planets, v.116 (E6), pp.E00G11.

Isaacson, P.J., Klima, R.L., Sunshine, J.M., Cheek, L.C., Pieters, C.M., Hiroi, T., Dyar, M. D., Lane, M., Bishop, J., (2014) Visible to near-infrared optical properties of pure synthetic olivine across the olivine solid solution. Amer. Mineral., v.99(2–3), pp.467–478.

Janardhan, A.S., Srikantappa, C. (1975)Geology of the northern parts of the Sargur schist belt between Mavinahalli and Doddakanya, Mysore district, Karnataka. Indian Mineral., v.16, pp.66–75.

Kloprogge, J.T., Frost, R.L., Rintoul, L. (1999) Single crystal Raman microscopic study of asbestos mineral chrysotile. Phys. Chem. Chem. Phys., v.1(10), pp.2559–2564.

Koukouzasa, N., Gemeni, V., Ziock, H.J. (2009) Sequestration of CO_2 in magnesium silicates, in Western Macedonia, Greece. Int. Jour. Miner. Process., v.93(2), pp.179-186.

Kuebler, K. E., Jolliff, B. L., Wang, A., Haskin, L. A. (2006) Extracting olivine (Fo–Fa) compositions from Raman spectral peak positions. Geochim. Cosmochim. Acta, v.70, pp.6201–6222.

Lazarev, Y. A. (1962) Line Broadening in Rotational and Rotation – Vibrational Raman Spectra of Gases. Opt. Spectrosc., v.13, pp. 373.

Lewis, I. R., Griffiths, P. R. (1996) Raman spectrometry with fiber-optic sampling. Appl. Spectrosc., v.50, pp.12A–30A.

McMillan, P. F., Hofmeister, A. M. (1988) Infrared and Raman spectroscopy. *In:* F.C. Hawthorne (Ed.), Spectroscopic Methods in Mineralogy and Geology, Review in Mineralogy, v.18, pp.99. Mineralogical Society of America, Washington, D. C.

Mernagh, T.P., Liu, L. (1991) Raman spectra from the Al_2SiO_5 polymorphs at high pressures and room temperature. Phys. Chem. Miner., v.18, pp.126–130.

Mohanty, J.K. (2009) Characterization of high magnesian rocks for suitability as flux in iron and steel industry. Jour. Geol. Min. Res., v.1(7), pp.149-155. doi: 10.5897/JGMR

Mondal, S.K., Mukherjee, R., Rosing, M.T., Frei, R., Waight, T., (2008) Petrologic, geochemical and isotopic study of 3.1Ga peridotite-chromitite suite from the western Dharwar craton (India): evidence for recycling of oceanic crust in the Mesoarchean. Eos Trans. AGU 89 (53) Fall Meet. Suppl., Abstract V33C-2237, AGU 2008 (San Francisco). (Abstract with programs).

Mukherjee, R., Mondal, S.K., Frei, R., Rosing, M.T., Waight, T.E., Zhong, H., Kumar, G.R.R. (2012) The 3.1 Ga Nuggihalli chromite deposits, Western Dharwar Craton (India): geo-chemical and isotopic constraints on mantle sources, crustal evolution and implications for supercontinent formation and ore mineralization. Lithos, v.155, pp.392–409.

Mukherjee, R., Mondal, S.K., Zhong, H., Bai, Z.J., Balaram, V., Kumar, G.R.R. (2014) Platinum-group element geochemistry of komatiite-derived 3.1 Ga ultramafic–mafic rocks and chromitites from the Nuggihalli greenstone belt, western Dharwar craton (India). Chem. Geol., v.386, pp.190–208.

O'Hanley, D., Dyar,M.D. (1998)The composition of chrysotile and its relationship with lizardite. Canad. Mineral., v.36 (3), pp.727–739.

Pathak, S., Dagar, A.K., Bhattacharya, S., Moitra, H., Chauhan, M., Saibal Gupta, S. (2021) Geological insights into lunar floor-fractured crater Atlas. Icarus, v.360, pp.114374.

Pasteris, J. D., Wopenka, B. (1987) Use of a laser Raman microprobe to trace geological reactions; in R.H. Geiss (eds) Microbeam Analysis-1987, San Francisco, San Francisco Press inc, pp.205-209.

Petriglieri, J.R., Salvioli-Mariani, E., Mantovani, L., Tribaudino, M., Lottici, P.P., Laporte-Magoni, C., Bersani, D. (2015) Micro-Raman mapping of the polymorphs of serpentine. Jour. Raman Spectrosc., v.46(10), pp.953–958.

Pichamuthu, C.S. (1962) Some observations on the structure, metamorphism, and geological evolution of Peninsular India. Jour. Geol. Soc. India (Online archive from Vol 1 to Vol 78), v.3, pp.106-118.

Pieters, C.M., Besse, S., Boardman, J., Buratti, B., Cheek, L., Clark, R.N., Combe, J.P., Dhingra, D., Goswami, J.N., Green, R.O., Head, J.W., Isaacson, P., Klima, R., Kramer, G., Lundeen, S., Malaret, E., McCord, T., Mustard, J., Nettles, J., Petro, N., Runyon, C., Staid, M., Sunshine, J., Taylor, L., Thaisen, K., Tompkins, S., Whitten, J. (2011). Mg-spinel lithology. A new rock type on the lunar farside. J. Geophys. Res. Planets, v.116 (E6), pp.E00G08.

Pieters, C.M., Hanna, K.D., Cheek, L., Dhingra, D., Prissel, T., Jackson, C., Moriarty, D., Parman, S., Taylor, L.A., 2014. The second conference on the Lunar highlands crust and new directions. The distribution of Mg-spinel across the Moon and constraints on crustal origin. Amer. Mineral., v.99, pp.1893–1910.

Prieto, A.C., Dubessy, J., Cathelineau, M. (1991) Structure-compo-sition relationships in trioctahedral chlorites: a vibrational spectroscopy study. Clays Clay Miner., v.39(5), pp.531–539.

Qureshy, M.N., Bhatla, S.C., Dlvakara Rao, V. (1970) Preliminary gravity studies over the ultramafics of Kadakola, Mysore (abstract). 2nd Symp. U.M.P., Hyderabad, India, pp.130.

Rao, V. D., Satyanarayana, K., Naqvi, S. M., Hussain, S. M. (1975) Geochemistry of Dharwar ultramafics and the Archaean mantle. Lithos, v.8(2), pp.77-91.

Rinaudo, C., Gastaldi, D., Belluso, E. (2003) Characterization of chrysotile, antigorite and lizardite by FT-Raman spectroscopy. Canad. Mineral., v.41(4), pp.883–890.

Rooney, J.S., Tarling, M.S., Smith, S.A.F., Gordon, K.C. (2018) Submicron Raman spectroscopy mapping of serpentinite fault rocks. Jour. Raman Spectrosc., v.49(2), pp.279-286.

Saikia, B.J., Parthasarathy G., Borah, R.R. (2017a) Nanodiamonds and silicate minerals in ordinary chondrites as determined by micro-Raman spectroscopy. Meteorit. Planet. Sci., v.52, pp.1146-1154.

Saikia, B.J., Parthasarathy, G., Borah, R.R., Satyanarayanan M., Borthakur, R., Chetia P. (2017b) Spectroscopy and mineralogy of a fresh meteorite fall Kamargaon (L6) chondrite. Proc. Indian Natl. Sci. Acad., v.83, pp.941-948.

Saikia, B.J., Parthasarathy, G., Borah, R.R., Borthakur, R., Sarmah, A.J.D. (2017c) Meteorite fall at Sadiya, India: A Raman spectroscopic classification. Jour. Astrophys. Aerosp. Tech., v.5(2), pp.1000149.

Saikia, B.J., Parthasarathy, G., Borah, R.R. (2018) Raman and Infrared Spectroscopic Tentative Identification of Organic Traces in Sadiya (LL5) Ordinary Chondrite. Advances in Astrophysics, v.3, pp.250-256.

Saikia, B.J., Parthasarathy,G., Gorbatsevich, F.F., Borah, R.R.(2021) Characterization of amphiboles from the Kola super-deep borehole, Russia by Raman and infrared spectroscopy. Geosci. Front., v.12(4), pp.101134.

Saikia, B.J., Parthasarathy, G., Chalapati Rao, N.V., Borah, R.R., Kumar, D. (2022a) High Shock Pressure Metamorphism Induced Transformations of Olivine and Feldspar in Natun Balijan L4 Chondrite: Evidence from Micro-Raman, Infrared Spectroscopy, X-ray Diffraction and Electron Microprobe Analysis. Jour. Geol. Soc. India, v.98, pp.731-739.

Saikia, B.J., Parthasarathy, G., Borah, R.R. (2022b) High-pressure polymorphs of olivine and silica in Kamargaon (L6) chondrite by laser micro-Raman and XRD studies. Jour. Earth Syst. Sci., v.131(1), pp.38-48.

Saikia, B.J., Parthasarathy, G., Borah, R.R. (2022c) Investigations of organic matter in meteorites using Fourier transform infrared and micro-Raman spectroscopic methods: Implications for origin of extraterrestrial organic matter. Jour. Indian Geophys. Union, v.26(1), pp.62-77

Sarkar, N.S., Kumar, T. N., Ray, D., Bhattacharya, S., Shukla, A.D., Moitra, H., Dagar, A., Chauhan, P., Sen, K., Das, S. (2019) Mineralogy and spectroscopy (VIS near infrared and micro-Raman) of chromite from Nidar

ophiolite complex, SE Ladakh, India: Implications for future planetary exploration. Planet. Space Sci., v.165, pp.1-9.

Sarkar, S., Bose, N., Bhattacharya, S., Bhandari, S. (2022), Identification of smectites by IR and LIBS instruments of Super Cam Suite onboard Mars 2020 Perseverance rover: comments on the Non-retrieval of First Drill Core. Curr. Sci., v.123(1), pp.93-96.

Srikantappa, C., Hörmann, P., Raith, M., (1984) Petrology and Geochemistry of Layered Ultramafic to Mafic Complexes from the Archaean Craton of Karnataka, Southern India. Archean Geochemistry, Springer, Berlin, pp.138–160.

Srikantappa, C., Raith, M., Ackermand, D. (1985) High-grade regional metamorphism of ultramafic and mafic rocks from the Archaean Sargur terrane, Karnataka, South India. Precambrian Res., v.30, pp.189–219.

Sharma, S. K., Angel, S. M., Ghosh, M., Hubble, H. W., Lucey, P. G. (2002) A remote pulsed-laser Raman spectroscopy system for mineral analysis on planetary surfaces to 66 meters. Appl. Spectrosc., v.56, pp.699-705.

Sharma, S. K., Lucey, P. G., Ghosh, M., Hubble, H. W., Horton, K. A. (2003) Stand-off Raman Spectroscopic Detection of Minerals on Planetary Surfaces, Spectrochim. Acta A, v.59, pp.2391-2407.

Stopar, J.D., Lucey, P.G., Sharma, S.K., Misra, A.K., Taylor, G.J., Hubble, H.W. (2005) Raman efficiencies of natural rocks and minerals: Performance of a remote Raman system for planetary exploration at a distance of 10 meters. Spectrochim. Acta A, v.61, pp.2315-2323.

Taylor, P.N., Chadwick, B., Friend, C.R.L., Moorbath, S., Ramakrishnan, M., Viswanatha, M.N. (1988) New age data on the geological evolution of Southern India. Jour. Geol. Soc. India, v.31, pp.155–157.

Titulaer, M.K., Vanmiltenburg, J.C., Jansen, J.B.H. and Geus, J.W. (1993) Characterization of Tubular Chrysotile by Thermoporometry, Nitrogen Sorption, Drifts, and TEM. Clays Clay Miner., v.41(4), pp.496-513.

Wang, A., Jolliff, B.L., Haskin, L.A., Kuebler, K.E., Viskupic, K.M. (2001) Characterization and comparison of structural and compositional features of planetary quadrilateral pyroxenes by Raman spectroscopy. Amer. Mineral., v.86, pp.790–806.

Yamamoto, S., Nakamura, R., Matsunaga, T., Ogawa, Y., Ishihara, Y., Morota, T., Hirata, N., Ohtake, M., Hiroi, T., Yokota, Y., Haruyama, J. (2010) Possible mantle origin of olivine around lunar impact basins detected by SELENE. Nat. Geosci., v.3, pp.533-536,